Research Square

Preprints are preliminary reports that have not undergone peer review.
They should not be considered conclusive, used to inform clinical practice,
or referenced by the media as validated information.

Comparative Study of Folded/Unfolded Peptide Dynamics with Modern AMBER Force Fields and Water Models

Marina Macchiagodena

marina.macchiagodena@unifi.it

Università degli Studi di Firenze https://orcid.org/0000-0002-3151-718X

Michele Casoria

Università degli Studi di Firenze

Anna Maria Papini

Università degli Studi di Firenze

Claudia Andreini

Università degli Studi di Firenze

Marco Pagliai

University of Florence

Piero Procacci

Università degli Studi di Firenze

Article

Keywords: AMBER, Water model, MD simulations, Folding, Unfolding, Secondary structure, DSSP, Peptide, Force Field, Benchmark

Posted Date: March 5th, 2026

DOI: https://doi.org/10.21203/rs.3.rs-8927435/v1

License: This work is licensed under a Creative Commons Attribution 4.0 International License.
Read Full License

Additional Declarations: There is **NO** Competing Interest.

Comparative Study of Folded/Unfolded Peptide Dynamics with Modern AMBER Force Fields and Water Models

Michele Casoria[1,2], Marina Macchiagodena[1*], Anna Maria Papini[1,2], Claudia Andreini[1,3], Marco Pagliai[1*], Piero Procacci[1*]

[1*]Dipartimento di Chimica "Ugo Schiff", Università degli Studi di Firenze, Via della Lastruccia 3-13, Sesto Fiorentino, I-50019, Italy.
[2]Interdepartmental Research Unit of Peptide and Protein Chemistry and Biology, Università degli Studi di Firenze, Via della Lastruccia 13, Sesto Fiorentino, I-50019, Italy.
[3]Magnetic Resonance Center (CERM), Università degli Studi di Firenze, Via Luigi Sacconi 6, Sesto Fiorentino, I-50019, Italy.

*Corresponding author(s). E-mail(s): marina.macchiagodena@unifi.it; marco.pagliai@unifi.it; piero.procacci@unifi.it;
Contributing authors: michele.casoria@unifi.it; annamaria.papini@unifi.it; claudia.andreini@unifi.it;

Abstract

Molecular dynamics simulations of biomolecules depend fundamentally on the accuracy of the force field and its interplay with the solvent model. The AMBER family is the preeminent and most reliable force field for protein simulations, yet its performance can vary significantly with different water models. This study presents an unprecedented assessment of this coupling, evaluating 95 AMBER-water model combinations through 117.75 microseconds of simulation on four peptides with both structured and disordered conformations. While many pairings capably reproduce ordered secondary structures, our systematic analysis reveals which combinations also faithfully capture the structural features of intrinsically disordered regions. The ff15ipq force field with TIP4P-D water model emerges as a particularly accurate pairing, though several other combinations

show significant promise. This comprehensive evaluation provides crucial guidance for selecting force fields that ensure high fidelity across diverse protein structural classes.

Keywords: AMBER, Water model, MD simulations, Folding, Unfolding, Secondary structure, DSSP, Peptide, Force Field, Benchmark

1 Introduction

Classical molecular force fields (FFs)[1] still rely on essentially the same empirical potential energy expressions first proposed by Lifson and Levitt in 1969.[2] These approaches are often referred to as *classical*, in contrast to *quantum*-mechanical methods. However, as Lifson himself argued[3] the core distinction between them is not rooted in classical versus quantum mechanics, but rather in methodology. Quantum-mechanical calculations are deductive, aiming to predict observable properties from first principles. Empirical and semiempirical methods, on the other hand, are inductive, seeking to formulate analytical expressions that reproduce observed phenomena.

Importantly, there is nothing inherently *classical* about empirical energy functions, as they are not derived directly from classical physics. Instead, they can be more accurately understood as empirical representations of the Born–Oppenheimer approximation.[4] Molecular dynamics (MD) simulation is now a widely used and powerful method to investigate biomolecular systems.[5–7] The quality of MD simulations is determined by the form of the functional, integration algorithm, extent of sampling, and FF, among which the FF is believed to be the most influential.[8, 9] Usually, the biomolecular systems are simulated in aqueous solutions; therefore, classical water models have become indispensable in atomistic simulations. Among all the models proposed over the years, rigid point-charge ones remain by far the most widely used.[10, 11]

Several major FF families have been developed in recent years; the key ones are AMBER,[12] CHARMM,[13] OPLS,[14] and GROMOS.[15] Among them, AMBER is the most used FF, as shown in Fig. S1 of Supplementary Information (SI), in which we analyzed all documents published from 1994 to 2025. Recently, the AMBER FFs have been comprehensively reviewed, with particular attention to the parameterization process.[16] The review traces the evolution of AMBER from its origins in the early 1980s to the key advancements that led to the widely adopted variants ff99SB-ILDN,[17] ff14SB,[18], and ff99SB.[19] Based on the information reported in the review, Fig. S2 in SI summarizes the derivation and relationships among AMBER FF versions, starting from ff94[20], which represents the first FF recommended for modern molecular dynamics simulations. For each FF, the corresponding recommended water model is also indicated (references for FFs: ff94,[20] ff96,[21] ff94gs,[22] ff-FB15,[23] ff14ipq,[24] ff15ipq,[25] ff99,[26] ff99ϕ,[27] ff03,[28] ff03w,[29] ff03*,[30] ff03cmap,[31] ff03ws,[32] ff99SB,[19] ff99SB-ϕ,[33] RSFF2,[34] RSFF2C,[35] RSFF2+,[36] ff99SBnmr1,[37],

ff99sbnmr1-ILDN,[17, 37] ff99SBnmr2,[38] ff99SB*,[30] ff99SB-ILDN,[17] ff99SB*-ILDN,[17, 30] ff99sb*-ILDN-Q,[39] ff99sb-ws,[32] ff99SBIDPs,[40] a99sb-disp,[41] DES-AMBER,[42] ff14SB,[18] ff19SB,[43] ff24EXP-GA,[44] ff14IDPs,[45] ff14IDPSFF,[46] ESFF1[47]).

Furthermore, Wang *et al.*[16] discuss the challenges that current FFs face in balancing protein–protein, protein–water, and water–water interactions in MD simulations, and examine possible strategies to overcome them. Optimizing water models and protein FFs to better approximate physical reality represents one of the most critical challenges for achieving balanced FFs. Nonetheless, this goal remains difficult to attain, with the main obstacle lying in the refinement of non-bonded parameters.

Encouragingly, recent years have witnessed the continuous development of high-quality water models. Most of these models rely on empirical adjustments derived from fitting experimental observations of diverse water properties, and they have proven capable of accurately reproducing a wide range of experimentally measurements.[48] The development of water models has been guided by the introduction of quantitative metrics and objective functions that capture their thermodynamic accuracy and enable systematic comparison between models.[49, 50] The optimization of non-bonded parameters has driven most recent advances. As a result, a consistent and transferable description of solute–solute, solute–solvent, and solvent–solvent interactions can only be achieved if the non-bonded parameters of biomolecular FFs reach an accuracy comparable to that of high-quality water models. In simulations of small peptides, the development of various FFs has often been driven by biases arising from differences in backbone parametrization, which can lead to the over-stabilization of specific secondary structures.[51, 52] Historically, particular water models have been favored in molecular simulations, typically for reasons of convention or compatibility with specific FF. Nevertheless, only a limited number of studies have systematically examined how simulation outcomes depend on the choice of water model.[53–55]

In our benchmark, we place particular emphasis on this aspect by systematically testing combinations of five different protein FFs (ff99SB-ILDN,[17] ff14SB,[18] ff19SB,[43] ff-FB15,[23] and ff15ipq[25]) with nineteen water models (SPC,[56] TIP3P,[57] SPC/E,[58] TIP3P-Ew,[59] SPC/E_b,[60] TIP3P-FB,[61] SPC/ϵ,[62] OPC3,[63] TIP3P-ST,[64] TIP4P,[57] TIP4P-Ew,[65] TIP4P/2005,[66] TIP4P-FB,[61] OPC,[67] TIP4P/ϵ,[68] TIP4P-D,[69] a99SB-disp,[41] TIP4P-ST,[64] and TIP4P-BG[70]) to assess their performance and mutual balance. While ff99SB-ILDN, ff14SB, and ff19SB are the most commonly used protein FFs, our benchmark also includes ff-FB15 and ff15ipq. The ff-FB15 FF incorporates energies and forces from high-level quantum mechanical calculations and adjusts all bonded parameters accordingly. In contrast, ff15ipq employs a novel method to derive atomic charges that explicitly accounts for solvent polarization effects.[25] Specifically, we selected four different peptides that are known to adopt either α-helical (PDB code: 1DJF and 1L2Y)[71, 72] or β-hairpin (PDB code: 2GB1(2-19) and 1GB1(41-56))[73] conformations and that display distinct stability or unfolding behavior in aqueous solution and we performed MD simulations using all the 95 FF-water model combinations for each one. In Table 1, a summary of the studied peptides is provided.

Table 1 Summary of the four peptides used in this study, including their sequence, structural motif, and experimental folding behavior. % deposited and % water indicate the % of peptide adopting the structural motif in the starting structure and in aqueous solution, respectively.

Peptide	PDB code	Sequence	Number of Residues	Structural motif	% deposited	% water
H1	1DJF	QAPAYKKAAKKLAES	15	α-helix	73%	5% [71]
H2	1L2Y	NLYIQWLKDGGPSSGRPPPS	20	α-helix	35%	35% [72]
B1	2GB1(2-19)	TYKLILNGKTLKGETTTE	16	β-hairpin	55%	5% [73, 74]
B2	2GB1(41-56)	GEWTYDDATKTFTVTE	16	β-hairpin	62%	25% [73, 75]

2 Results

For each peptide, we analyzed the results obtained for all simulated FF-water model combinations. As will be shown, the outcome depends on the choice of the FF. Moreover, significant variations are also observed depending on the specific water model combined with the FF, with the best performance achieved using the TIP4P-D water model. In the following, we present a discussion of the results obtained for all FF-water model combinations, with more detail for this particular water model in combination with ff15ipq FF. The results for all 95 FF-water model combinations can be interactively navigated and analyzed in the accompanying GitHub repository at https://marinamacchiagodena.github.io/AMBERFFs-WaterModels/. In Figures S3-S6 of the SI we provided basic guidance for navigation.

2.1 The H1 Peptide

H1 displays 73% α-helical content in the starting 1DJF PDB structure (derived from an NMR study performed in sodium dodecyl sulfate), whereas it has been reported to be poorly structured in aqueous solution (5%, Tab. 1). Characterized by a +4 e net charge, the H1 peptide sequence includes two Lys-Lys repeats interrupted by an Ala-Ala motif. The considerable electrostatic repulsion arising from these contiguous Lys-Lys dyads, along with a helix-disrupting proline at position 3, are key destabilizing elements that point to very fast unfolding, on the order of nanoseconds.

Across almost all replicates (20 ns $\times$ 15), the helical content of the ff15ipq-TIP4P-D combination (as measured by the DSSP analysis, Fig. 1(a)) decreases within the first few nanoseconds. By collecting the helical content in each simulation frame and subdividing the trajectories into nanosecond intervals, we were able to characterize the unfolding process (Fig. 1(c)) in all 15 MD simulations, averaging the results. Using the ff15ipq FF in combination with the TIP4P-D water model, the initial helical content ($\approx$ 70%) decreases to 25% in just 6 ns. The peptide reaches a fully unfolded state within approximately 15 ns. The widely used ff99SB-ILDN FF combined with the TIP4P-D water model displays similar behavior, exhibiting an unfolding time ($\approx$10 ns) even faster than that observed with ff15ipq. Notably, the ff19SB/TIP4P-D combination - despite incorporating quantum mechanics-derived two-dimensional CMAP corrections for the ϕ-ψ dihedral angles - appears to overstabilize the H1 helix, maintaining more

than 50% helical content at 20 ns without observable unfolding. To ensure that the five FFs, in combination with all water models, do not stabilize other structural motifs, we analyzed all secondary structures obtained from the DSSP output files. The results are reported in Figs. S7–S11 of the SI and show that the predominant structural motif is the α-helix for all combinations, confirming that our analysis is robust.

Analysis using the DSSE metric indicates a low entropy for the N-terminal residues, due to the initial coil state in the experimental structure (Fig. 1(b)) for all five FF-TIP4P-D combinations. Instead, the DSSE values for the central region allow us to value the FFs' performance: ff99SB-ILDN, ff15ipq, and ff-FB15 have higher DSSE values than ff14SB and ff19SB, suggesting that from the simulations performed using the last FFs, the residues are stably folded and close to the starting structure, failing to describe the unfolding process properly.

Finally, we quantified the deviation of the helical content from the experimental finding of 5% (see Tab. 1) in the last nanosecond of each simulation for all FF–water model combinations. The results are summarized in Fig. 1(d). The choice of FF exerts the strongest influence on the results, while the selected water model slightly modulates the trends imposed by it. The best agreement with experiment is obtained using ff99SB-ILDN and ff15ipq, both of which correctly predict the unfolding process within 20 ns. In contrast, ff14SB and the newest version, ff19SB, fail to capture peptide unfolding across all water models. Ff-FB15 provides intermediate results, with a stronger dependence on the specific water model employed.

Among the 3-site water models examined, the SPC model yields the highest accuracy, while within the TIP3P family, TIP3P-EW performs best. For the 4-site water models, the results are generally more consistent and accurate overall, with the TIP4P-D model providing the closest agreement with experimental helical content. The use of the TIP4P-D water model also improves the results obtained with ff-FB15 FF, for which the deviation from the experimental finding drops to a value of 5.0%.

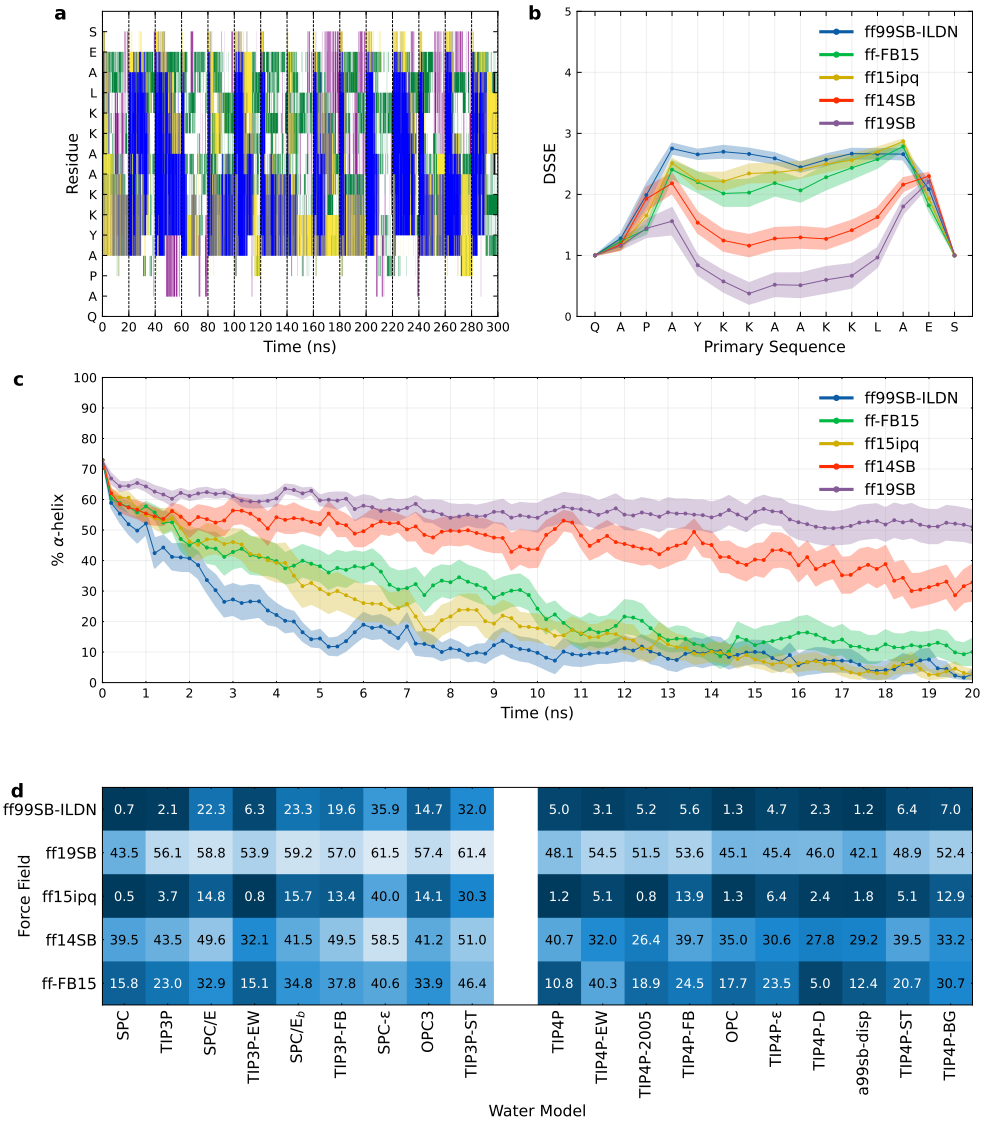


Fig. 1 **a**: H1 DSSP calculated from the 15 molecular dynamics simulations of 20 ns each (300 ns in total), with ff15ipq-TIP4P-D water model combination. Color code: blue, α-helix; green, bent; yellow, turn; violet, π-helix; gray: 3-helix; white: coil. **b**: H1 DSSE calculated from 15 repetitions with the five FFs-TIP4P-D water model combinations: in blue, ff99SB-ILDN; in green, ff-FB15; in yellow, ff15ipq; in red, ff14SB; and in violet, ff19SB. The shaded area represents the error computed with bootstrap resampling. **c**: H1 unfolding process calculated for the five FFs-TIP4P-D water model combinations by averaging the DSSP results of the 15 MD simulations, each of 20 ns. On the y-axis, the percentage of α-helix, and on the x-axis, the time in ns. In blue, ff99SB-ILDN; in green, ff-FB15; in yellow, ff15ipq; in red, ff14SB; and in violet, ff19SB. The shaded area represents the error computed with bootstrap resampling. **d**: H1 heatmap showing the deviation of the final helical content (in %) from the experimental findings (see Tab. 1) using different FF-water model combinations. Agreement with the experiment increases with the intensity of the blue color.

2.2 The H2 Peptide

H2 is a Trp-cage miniprotein known for its stability in aqueous solution. It derives from the truncation and mutation of a poorly folded 39-residue peptide, resulting in a 20-residue construct that is over 95% folded in water at physiological pH.[72] This construct adopts a novel and highly stable fold characterized by cooperative, hydrophobically driven encapsulation of a Trp side chain within a sheath of Pro rings. The experimental folded structure displays a helical content of approximately 35% (see Tab. 1). Comparable results are obtained from MD simulations. Indeed, as shown by the DSSP and the unfolding process reported in Figs. 2(a) and 2(c), respectively, the H2 peptide remains stable during all 15 MD replicates. The α-helix is present in every nanosecond of all 15 simulations. Analyzing Fig. 2(c) in detail, the native conformer population, with a 35% content of α-helix, is firmly maintained for all five FFs in combination with the TIP4P-D water model. Furthermore, H2 does not adopt any other predominant structural motifs, as shown in Figs. S7–S11 of the SI.

Regarding the DSSE analysis shown in Fig. 2(b), the C-terminal region, where the Pro residues are located, exhibits higher mobility, with a tendency that increases linearly with the chosen FF, from ff14SB to ff-FB15. The first region, from the N-terminal to the tenth residue, presents DSSE values that are very low, except for the second and ninth residues. The values are comparable for all the tested FFs, suggesting that their performance in reproducing the folding process is comparable. From the heatmap in Fig. 2(d), it is evident that all combinations are generally consistent, with minor variations arising from the water model. The deviation from the experimental findings is usually less than 3%, except for ff99SB-ILDN in combination with TIP3P, SPC/E, and a99sb-disp, and for ff15ipq in combination with a99sb-disp.

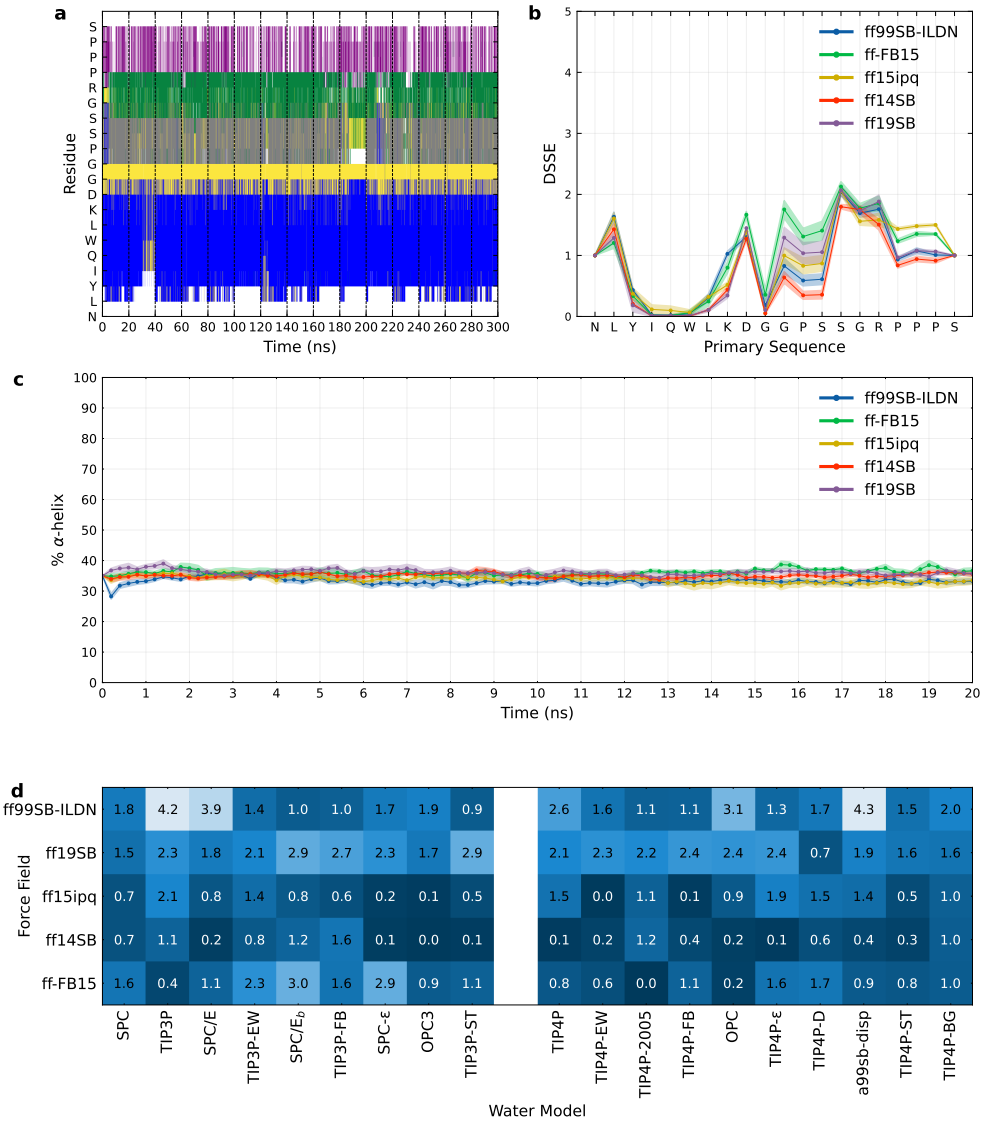


Fig. 2 **a**: H2 DSSP calculated from the 15 molecular dynamics simulations of 20 ns each (300 ns in total), with ff15ipq-TIP4P-D water model combination. Color code: white, coil; blue, α-helix; green, bent; yellow, turn; violet, π-helix; gray: 3-helix. **b**: H2 DSSE calculated from the 15 repetitions with the five FFs-TIP4P-D water model combinations: in blue, ff99SB-ILDN; in green, ff-FB15; in yellow, ff15ipq; in red, ff14SB; and in violet, ff19SB. The shaded area represents the error computed with bootstrap resampling. **c**: H2 unfolding process calculated for the five FFs-TIP4P-D water model combinations by averaging the DSSP results of the 15 MD simulations, each of 20 ns. On the y-axis, the percentage of α-helix, and on the x-axis, the time in ns. In in blue, ff99SB-ILDN; in green, ff-FB15; in yellow, ff15ipq; in red, ff14SB; and in violet, ff19SB. The shaded area represents the error computed with bootstrap resampling. **d**: H2 heatmap showing the deviation of the final helical content (in %) from the experimental findings (see Tab. 1) using different FF-water model combinations. Agreement with the experiment increases with the intensity of the blue color.

2.3 The G-protein Derived B1 and B2 Peptides

B1 and B2, which adopt β-hairpin motifs, are both derived from the same protein but exhibit distinct conformational behaviors, as discussed in the Method Section.
B1: This sequence originates from the N-terminal fragment; in the starting PDB structure, the two antiparallel β-sheets involve residues 2–6 and 13–17, accounting for 55% of the peptide. On the other hand, the isolated 2-19 fragment is known experimentally to be largely unstructured in aqueous solution (see Tab. 1), making it a stringent test case for assessing spurious secondary-structure stabilization in MD simulations. In the B1 sequence, the NGKT turn is suboptimal, thereby reducing stability. Moreover, B1 exhibits a limited hydrophobic core with only five hydrophobic residues that are not well-paired, along with a high glycine content that increases backbone flexibility while reducing β-strand propensity. Using a two-state (folded–unfolded) approximation and taking the free energy (ΔG) difference between the folded (f) and unfolded (u) states $\Delta G = RT \ln(k_u/k_f) \approx +2$ kcal/mol based on experimental data (see Tab. 1), we can estimate the unfolding time $1/k_u$ for B1 to be in the range $\approx 30 - 40$ ns, where we have adopted a typical β-hairpin folding rate $k_f = 10^6$ s^{-1}.

As shown in Fig. 3(a) for the ff15ipq–TIP4P-D combination, the two β-strands unfold in distinct regions during the simulations. Initially, their combined length increases, covering approximately 65% of the peptide, before gradually decreasing during unfolding. The unfolding pathway varies across the 15 independent MD replicates. By averaging the DSSP-derived β-sheet content over all trajectories, we observe a monotonic decrease from the initial ≈65% to ≈30% after 20 ns (see Fig.3(c)). This behavior aligns with the estimated unfolding time of 30–40 ns for B1. Reliability of the ff15ipq-TIP4P-D combination in describing B1 is further supported by the data reported in Fig. S12 of the SI, which refers the unfolding process at higher temperature (340 K). In this case, the β-sheet content, averaged over 15 independent 50 ns MD simulations, decreases to ≈5% after 20 ns, arriving at a completely unfolded structure after 30 ns. Instead, the β-sheet content calculated using the other four FFs in combinations with the TIP4P-D water model remains high, especially with ff-FB15. Furthermore, we have verified that B1 does not adopt any other predominant structural motifs, as shown in Figs. S7–S11 of the SI.

DSSE analysis (Fig. 3(b)) further indicates persistent β-sheet structure in the central regions (residues 4–5, 9–10, 14–15), consistent with experimental observations of low-populated chain bends at residues 8–9 and 14–15. For these residues, the DSSE values are higher for ff15ipq FF and lower when ff-FB15 FF is used. For all other residues, DSSE values are quite high, and the ff15ipq FF shows the highest values. As illustrated by the B1 heatmap of Fig. 3(d), several FF-water model combinations show a mismatch with the experimental data; in these cases, the FFs tend to over-stabilize the peptide, with only a negligible fraction adopting the correct β-hairpin conformation. The over-stabilization effect is more evident when 3-site water models are used, and with ff-FB15. In this last case, the over-stabilization is also present in combination with 4-site water models. Ff14SB-TIP4P-ST combination exhibits a deviation of 24.1%, resulting in the best overall agreement. Deviations below 30% are also observed for ff14SB combined with OPC and TIP4P-ϵ water models. In addition, encouraging results are obtained with TIP4P-D and a99sb-disp water models. Very

good results are also obtained with ff15ipq in combination with TIP4P-D and a99sb-ildn; in the former case, the deviation is of 29.5%.

B2: This sequence corresponds to the second β-hairpin of the B1 domain of protein G. As reported in Tab. 1, it adopts a population containing up to 40% native-like β-hairpin structure in pure water under standard conditions. The unfolding time at 297 K has been estimated via nanosecond laser temperature-jump experiments to be on the order of microseconds.[76]

The initial PDB structure 2GB1(41–56) features β-sheets spanning residues 2–6 and 11–15, covering 62% of the peptide length. DSSP analysis in Fig. 4(a) confirms the stability of this fold in simulations using the ff15ipq–TIP4P-D combination. The hairpin remains stable throughout nearly all 15 independent MD replicates. Furthermore, we have verified that B2 does not adopt any other predominant structural motifs, as shown in Figs. S7–S11 of the SI. During the slow unfolding process (Fig. 4(c)), the native-like conformation persists after 20 ns at approximately 70–75% for all FFs–TIP4P-D combinations, corresponding to a β-sheet content of 40–50%. In all cases, the overall hairpin architecture is conserved, with only minor fraying observed at the initial antiparallel β-sheet ends, as also indicated by the DSSE profile in Fig. 4(b). Since peptide B2 is known to unfold on the μs timescale, while our initial simulations were limited to 20 ns, we performed additional tests on the five FFs using the TIP4P-D water model. We then ran 15 repetitions of 50 ns simulations each, at an elevated temperature (340 K). At this temperature, the observed folding population is close to 10%,[76] in agreement with experimental estimates. These higher-temperature simulations better discriminate among the FFs under identical solvent conditions. In particular, ff15ipq and ff99SB-ILDN reproduce the expected behavior, with B2 predominantly unfolded at 340 K. By contrast, the other FFs tend to overstabilize the folded state, leading to comparatively high residual folding populations (see Fig. S13 of SI).

Notably, we consistently observe across all FFs a higher DSSE in the N- and C-terminal regions and a low DSSE value in the central turn region, which is stabilized by the hydrophobic cluster W–Y–F–W. This pattern aligns well with the observation that "in the native fold the molecular species contain the complete hydrophobic cluster, with the most populated species having frayed ends."[76]

For the ff15ipq–TIP4P-D combination, partial unfolding in standard conditions appears slightly faster compared to other TIP4P-D–based models. The β-sheet percentage averaged over 15 simulations drops to about 39% at 20 ns, representing a 13.6% deviation from the reference equilibrium value (see Table 1 and Fig. 4(d)). The unfolding process is likely driven by an initial rapid decay due to the breaking of hydrogen bonds (HBs) connecting the terminal regions, followed by a much slower decay to equilibrium that involves the disruption of the central hydrophobic cluster.

Considering all other FFs–water model combinations (Fig. 4(d)), we generally observe structural stabilization, with β-sheet content exceeding 40% in most cases. For ff14SB, ff15ipq, and ff99SB-ILDN combined with 3-site water models, we observe a degree of over-stabilization, with β-sheet percentages near or above 50%, corresponding to a deviation from the 25% target value of approximately 25 percentage points. The same trend holds for ff14SB and ff99SB-ILDN combined with 4-site water models.

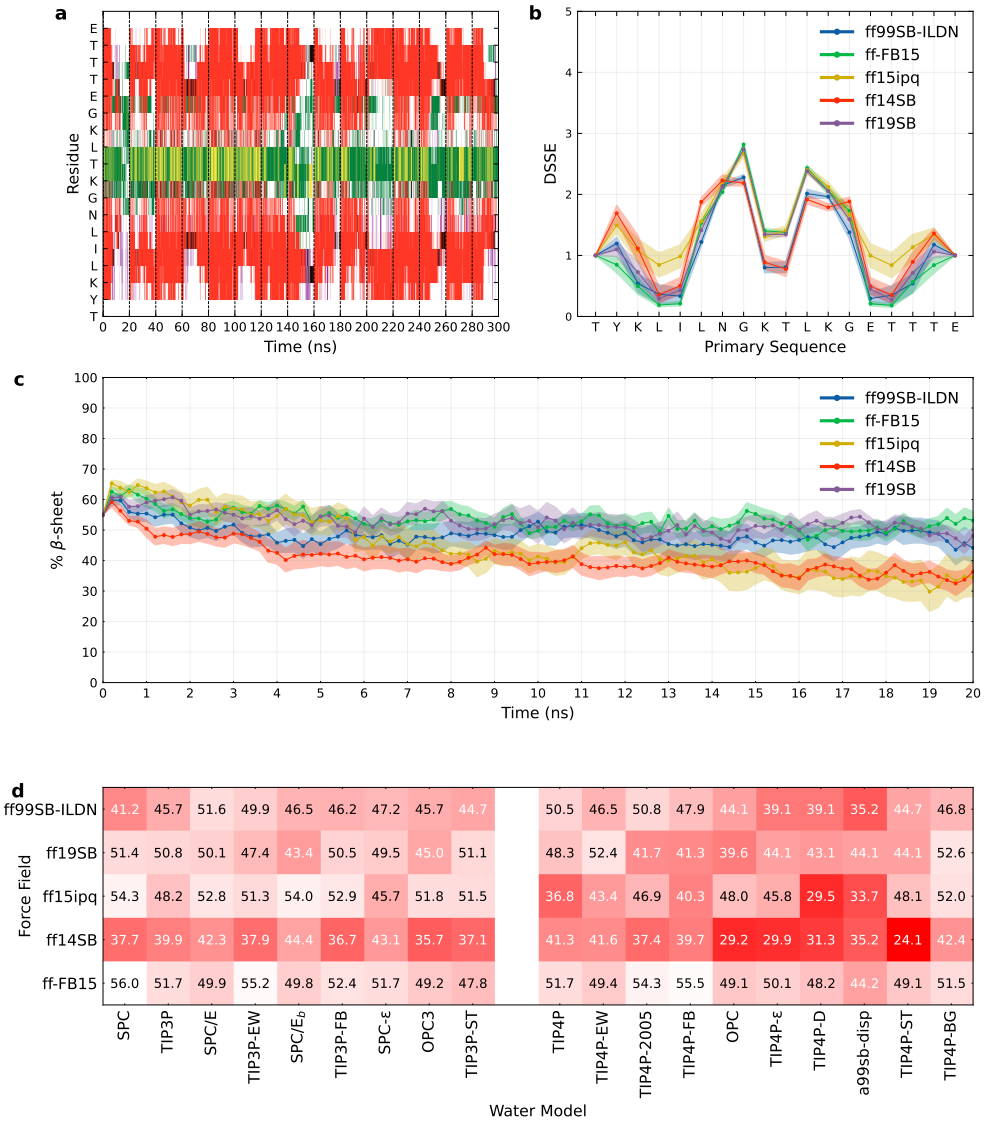


Fig. 3 **a**: B1 DSSP calculated from the 15 molecular dynamics simulations of 20 ns each (300 ns in total), with ff15ipq-TIP4P-D water model combination. Color Code: white, coil; red, β-strand; green, bent; yellow, turn; violet, π-helix; black: β-bridge. **b**: B1 DSSE calculated from 15 repetitions with the five FFs-TIP4P-D water model combinations: in blue, ff99SB-ILDN; in green, ff-FB15; in yellow, ff15ipq; in red, ff14SB; and in violet, ff19SB. The shaded area represents the error computed with bootstrap resampling. **c**: B1 unfolding process calculated for the five FFs-TIP4P-D water model combinations by averaging the DSSP results of the 15 MD simulations, each of 20 ns. On the y-axis, the percentage of β-sheet, and on the x-axis, the time in ns. In in blue, ff99SB-ILDN; in green, ff-FB15; in yellow, ff15ipq; in red, ff14SB; and in violet, ff19SB. The shaded area represents the error computed with bootstrap resampling. **d**: B1 heatmap showing the deviation of the final β-sheet content (in %) from the experimental findings (see Tab. 1) using different FF-water model combinations. Agreement with the experiment increases with the intensity of the red color.

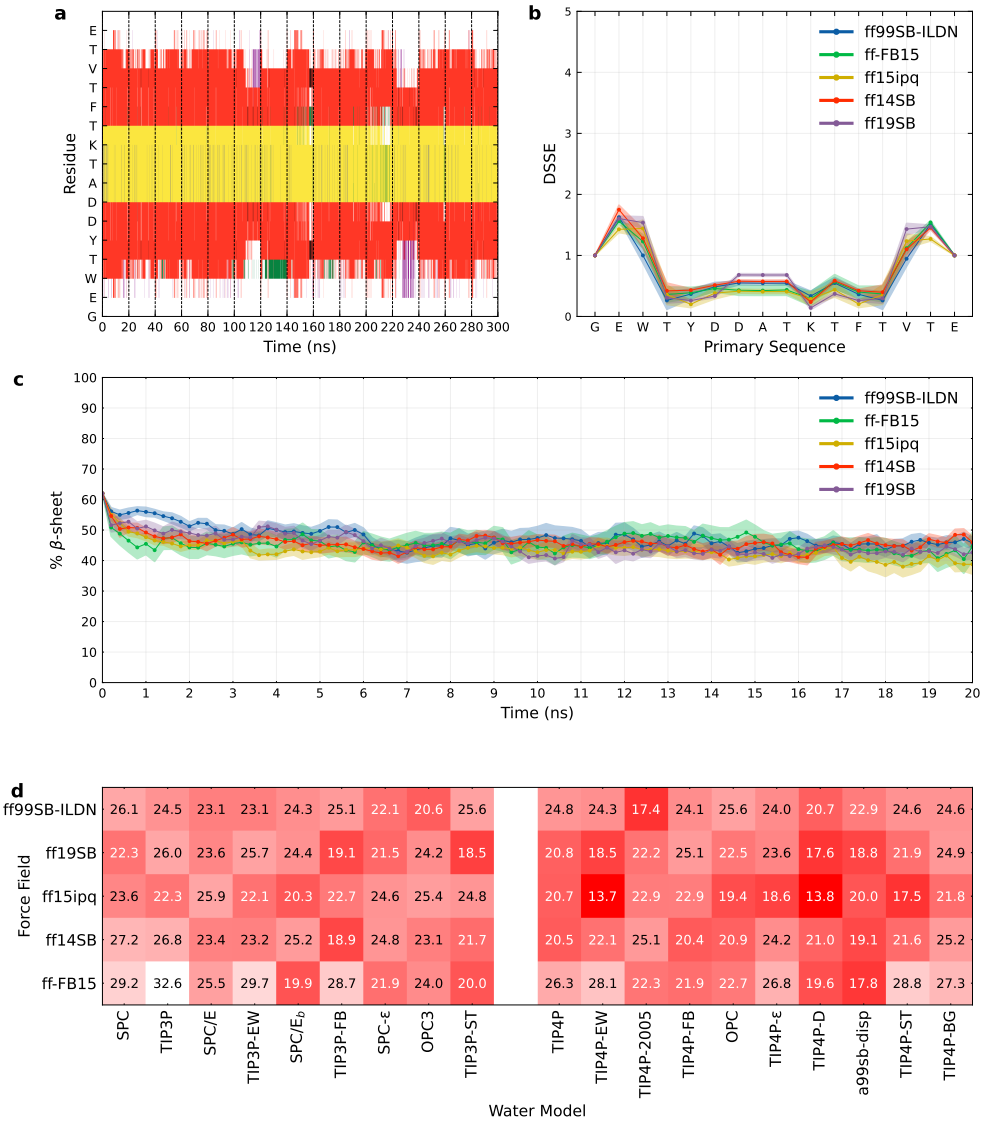


Fig. 4 **a**: B2 DSSP calculated from the 15 molecular dynamics simulations of 20 ns each (300 ns in total), with ff15ipq-TIP4P-D water model combination. Color Code: white, coil; red, β-strand; green, bent; yellow, turn; violet, π-helix; black: β-bridge. **b**: B2 DSSE calculated from the 15 repetitions with the five FFs-TIP4P-D water model combinations: in blue, ff99SB-ILDN; in green, ff-FB15; in yellow, ff15ipq; in red, ff14SB; and in violet, ff19SB. The shaded area represents the error computed with bootstrap resampling. **c**: B2 unfolding process calculated for the five FFs-TIP4P-D water model combinations by averaging the DSSP results of the 15 MD simulations, each of 20 ns. On the y-axis, the percentage of helicity, and on the x-axis, the time in ns. In blue, ff99SB-ILDN; in green, ff-FB15; in yellow, ff15ipq; in red, ff14SB; and in violet, ff19SB. The shaded area represents the error computed with bootstrap resampling. **d**: B2 heatmap showing the deviation of the final β-sheet content (in %) from the experimental findings (see Tab. 1) using different FF-water model combinations. Agreement with the experiment increases with the intensity of the red color.

3 Methods

3.1 The Force Field

The functional form of FFs can be expressed as $\phi[V_{\text{total}}(r_{ij}), \mathbf{J}]$, where $\mathbf{J}$ is an $n \times p$ matrix containing P parameters for N atoms.

An example of such a functional is:

$$\begin{aligned}\phi[V_{\text{total}}(r_{ij}), \mathbf{J}] = {} & V_{\text{bond}}\left(r_{ij}, \{k_{ij}^{\text{bond}}, r_{ij}^{\text{eq}}\}\right) + V_{\text{angle}}\left(r_{ij}, \{k_{ijk}^{\text{angle}}, \theta_{ijk}^{\text{eq}}\}\right) \\ & + V_{\text{dihedral}}\left(r_{ij}, \{k_{ijkl}^{\text{dih}}, n\}\right) + V_{\text{vdW}}\left(r_{ij}, \{\sigma_{ij}, \varepsilon_{ij}\}\right) \\ & + V_{\text{elec}}\left(r_{ij}, \{q_{ij}\}\right)\end{aligned}$$

In practice, only a limited number of parameters is required. Instead of assigning individual parameters to each of the N atoms in a molecule, atoms are grouped into general m *atom types*. As a result, only $m < N$ unique parameter sets are defined.

For non-bonded interactions, the Lennard-Jones (LJ) potential for van der Waals (VDW) interactions and the Coulomb potential are commonly employed. This necessitates the use of fixed atomic charges. Importantly, the LJ parameters σ_{ij} and ε_{ij} are not stored explicitly for every atom pair. Instead, they are calculated from atomic parameters σ_i, σ_j, ε_i, and ε_j through specific mixing rules. In the AMBER FF, the Lorentz–Berthelot (LB) combination rules [77, 78] are applied:

$$\sigma_{ij}^{LB} = \frac{\sigma_i + \sigma_j}{2}$$
$$\varepsilon_{ij}^{LB} = \sqrt{\varepsilon_i \cdot \varepsilon_j}$$

Furthermore, 1–4 non-bonded interactions are not applied at their full strength; both the LJ and Coulomb contributions are scaled by predefined factors. In this context, FF refers to fixed-charge additive FFs within the AMBER framework.

3.2 The Model Systems

The four peptides selected as model systems to evaluate the performance of different FF–water model combinations are reported in Table 1, which summarizes their main characteristics, including sequence, structural motif, and experimentally observed folding behavior in starting structure and in aqueous solution. Two of them, H1 and H2, are α-helical peptides, yet they display markedly different stability and helical populations in water.[71, 72] H1 is derived from residues 56–70 of human platelet factor 4 (PF4), where most Ile and Leu residues were replaced by Ala, resulting in a highly basic variant. Circular dichroism spectra at physiological pH indicate that H1 predominantly adopts disordered conformations, consistent with a random-coil signature in solution. In contrast, H2 is a Trp-cage peptide, a well-characterized motif containing a compact hydrophobic core centered around a buried tryptophan residue, known to exhibit significant structural stability and pronounced α-helical content in aqueous environments.

The remaining two peptides, B1 and B2, correspond to β-hairpin motifs, consisting of a β-turn connecting two strands of an antiparallel β-sheet within the

immunoglobulin-binding domain.[73] They exhibit distinct folding propensities in aqueous solution. For B1, circular dichroism spectra indicate that the peptide behaves as a flexible chain in water, with no clear signatures of a significantly populated folded structure. NMR data corroborate this observation, revealing predominantly extended conformations with only minor populations of folded states.[74] In contrast, the far-UV CD spectrum of B2 displays a minimum near 200 nm and a maximum around 186 nm, consistent with the presence of some secondary structure in equilibrium with random-coil conformations. Quantitative analysis estimates that approximately 42% of the peptide preserves the native fold in solution, with the turn region being particularly stable, based on conformational shifts similar to those observed in native protein.[75] In Table 1, we report the relative percentages of secondary structure in water and in the starting structure, as expected based on experimental observations.

3.3 Force Fields-Water Model Combinations

The benchmark includes five protein FFs: ff99SB-ILDN,[17] ff14SB,[18] ff19SB,[43] FB15,[23] and ff15ipq[25] and nineteen water models. All possible pairwise combinations were evaluated, yielding 95 distinct simulation setups, to assess the combined effect of peptide parametrization and water representation on the computed properties. The water models cover both 3-site and 4-site types, ranging from established ones such as TIP3P, TIP4P,[57], and SPC[56] to more recent parametrizations like TIP3P-ST[64] and TIP4P-BG.[70] A complete summary of the selected 3-site and 4-site models is provided in Tables S1 and S2 of the SI, respectively. Furthermore, to highlight the differences between the geometric and electrostatic parameters of the water models, in Fig. S14 of the SI, we reported two radar plots, one for each model type.

3.4 Molecular Dynamics Simulations

Our methodology is based on *ensemble simulations*,[79] comprising 15 independent replicates of 20 ns each. The replicates differ only in their initial conditions (e.g., initial velocities). By increasing the likelihood of rare events, such as conformational transitions, this strategy enables standard molecular dynamics simulations to achieve effectively enhanced conformational sampling.[80, 81] In this benchmark, all replicas share the same initial configuration, while their initial velocities were independently drawn from a Maxwell-Boltzmann distribution.

All simulations were conducted in a cubic box with periodic boundary conditions using GROMACS 2025.1.[82] To build the topology files, the standard tLEaP[83] and ParmEd[84] tools are used, fixing the known bug for ff19SB's CMAPs inclusion. Each system was first subjected to energy minimization using the steepest descent algorithm. The minimized configuration then served as the starting point for an NPT equilibration (298.15 K and 1 atm, 100 ps, time-step 1 fs), employing the C-rescale exponential relaxation pressure coupling with a characteristic pressure fluctuation period of 2 ps and a V-rescale thermostat [85] with a coupling constant of 1 ps, until the systems reached a stationary density value, averaged over 5 ps time windows.

Production runs in the NPT ensemble (298.15 K and 1 atm) were performed for 20 ns with a time-step of 2.0 fs, applying rigid constraints only to X-H bonds (with X representing any heavy atom) via the LINCS algorithm.[86] Electrostatic interactions were treated using the particle-mesh Ewald (PME) method[87] with a grid spacing of 1.2 Å, a real-space cutoff of 1.2 nm, and fourth-order spline interpolation. Van der Waals interactions were computed with a cutoff of 1.0 nm, including long-range dispersion corrections for energy and pressure.[82, 88]

This protocol yields a total of 300 ns per system combination, corresponding to 28.5 μs of cumulative simulation time for each peptide, and a total simulation time of 114 μs.

Furthermore, for B1 and B2 systems, we performed additional production runs in the NPT ensemble, keeping the temperature at 340 K, for 15 independent replicates of 50 ns each. These auxiliary simulations were performed for the five FFs/TIP4P-D water model combinations corresponding to an additional 3.75 μs simulation time.

3.5 Analysis

To assess the ability of different FF–water model combinations to reproduce peptide structural behavior, we developed a benchmarking protocol that evaluates both conformational stability and flexibility over MD trajectories. Using the Define Secondary Structure of Proteins (DSSP) algorithm[89, 90], each frame of the trajectory was analyzed to determine the percentage of secondary structure elements. The analysis was carried out by tracking, for each frame, the fraction of residues adopting α-helical or β-sheet conformation, indicated with H and E for one-symbol secondary structure designations in output files, respectively. By averaging these values over all simulation replicas, we obtained a smooth description of the structural trends. This approach allows us to evaluate the stability of the secondary structure throughout the trajectory and to detect possible transitions between folded and unfolded states. Regions showing persistently high helical content indicate structural stability. The resulting structural populations were then compared with experimental reported values, providing a direct measure of the agreement between simulations and experimental observations. Furthermore, since DSSP analysis enables the identification of additional secondary structure elements, beyond H and E, we examined all of them to be sure that the FF/water model combinations do not stabilize any alternative structural motifs.

We introduce a novel per-residue descriptor, DSSE (DSSP-based Secondary Structure Entropy), which integrates two complementary measures: (i) the conformational variability of each residue over time, and (ii) the deviation of its structural behavior from the experimentally determined reference. These properties are quantified using secondary structure information extracted via the `DSSP` algorithm, which assigns one of nine discrete secondary structure classes (e.g., α-helix, β-sheet, turn, coil) to each residue in each simulation frame. To capture local flexibility, we compute the Entropy (S) of the DSSP state distribution for each residue i:

$$S_i = -\sum_{j=1}^{9} p_{ij} \log_2 p_{ij} \tag{1}$$

where p_{ij} is the frequency of DSSP state j for residue i across the trajectory. Low entropy indicates structural stability (e.g., consistent α-helical conformation), whereas high entropy reflects structural fluctuation or disorder.

To assess structural fidelity, we compare the per-frame DSSP assignments with the reference secondary structure, using a normalized similarity score. For each residue, we compute the proportion of frames in which the simulated secondary structure matches the reference:

$$\mathrm{Sim}_i = \frac{1}{T} \sum_{t=1}^{T} \delta(s_i^{(t)}, s_i^{\mathrm{ref}}) \tag{2}$$

where $s_i^{(t)}$ is the DSSP state of residue i at time t, s_i^{ref} is the corresponding state in the reference structure, and δ is the Kronecker delta.

The final DSSE score for each residue is computed by combining structural entropy with deviation from the reference:

$$\mathrm{DSSE}_i = S_i + (1 - \mathrm{Sim}_i) \tag{3}$$

This combined metric allows us to distinguish between residues that are stably folded and close to the reference structure (low DSSE) and those that are either structurally flexible or poorly aligned with the experimental model (high DSSE).

Implementation was performed in a batch-wise manner over 15 simulation replicas, three batches of 5 replicas each, per peptide. For each trajectory, DSSP values were extracted. This framework supports robust benchmarking of AMBER FFs with water model combinations at residue-level resolution, enabling the identification of simulation protocols that best preserve native-like peptide folding behavior.

For each FF and water model combination, an error metric was computed to quantify the deviation from the assigned target values for each peptide. Given a target value T_p and the corresponding simulation output $S_{ff,wm}^{(p)}$, the error for peptide p is defined as the absolute difference:

$$e_p^{\mathrm{FF,W}} = \left| S_{ff,wm}^{(p)} - T_p \right|$$

The overall error associated with the (FF, W) combination is then obtained by averaging the individual errors:

$$E^{\mathrm{FF,W}} = \frac{1}{N_p} \sum_{p=1}^{N} e_p^{\mathrm{FF,W}}$$

where N_p is the number of peptides studied (four in our case). This error value represents the average deviation from the target values, Mean Absolute Error (MAE) reported in Fig. 5.

To investigate how water model parameters influence peptide stability, we focused on unstructured peptides (H1 and B1). For each peptide p, we defined the peptide-specific mean $P_s^{(p)}$, computed across all FFs and water models as defined in Equation 4:

$$P_s^{(p)} = \frac{1}{N_{ff} N_{wm}} \sum_{ff=1}^{N_{ff}} \sum_{wm=1}^{N_{wm}} S_{ff,wm}^{(p)} \tag{4}$$

where N_{ff} and N_{wm} are the number of FFs and water model respectively. This procedure removes intrinsic differences between peptides and isolates relative stability changes induced by the water model.

The relative stability $\Delta S_{ff,wm}^{(p)}$ of each peptide in a specific simulation with water model and FF is then defined as the difference from respective peptide-specific mean:

$$\Delta S_{ff,wm}^{(p)} = S_{ff,wm}^{(p)} - P_s^{(p)} \tag{5}$$

Finally, we computed the average relative stability $\overline{\Delta S}$ over all peptides:

$$\overline{\Delta S} = \frac{1}{N_p} \sum_{p=1}^{N_p} \Delta S_{ff,wm}^{(p)} \tag{6}$$

where N_p is the number of peptides considered (two in this case, H1 and B1). This average relative stability, $\overline{\Delta S}$, represents the averaged over all peptides and FFs and is considered as a function of the water model parameters (dipole moment μ, Lennard–Jones σ, and ϵ) reported in Tab. S3-S4. Multivariate linear regression was performed using these parameters of each water model as predictors. Continuous predictors were standardized (zero mean, unit variance) to allow direct comparison of effect sizes. Regression coefficients (β) therefore quantify the estimated change in relative peptide stability associated with a one–standard deviation variation of each parameter.

Because multiple simulations share the same water model parameters, observations are not fully independent. To account for this, standard errors were estimated by clustering observations at the water-model level. This approach acknowledges that simulations using the same water model may be correlated and yields more reliable and conservative uncertainty estimates. Statistical analyses were performed using the Python library *statsmodels*. [91]

4 Discussion

The combined effect of the FF and the associated solvent model determines peptide conformational equilibrium. Historically, different protein FFs have been developed and validated in conjunction with specific water models: ff99SB-ILDN and ff14SB are commonly paired with TIP3P, ff19SB was optimized together with OPC, while ff15ipq and ff-FB15 rely on distinct, internally consistent solvent representations. In this context, assessing the transferability of FFs across multiple water models provides a unified framework for identifying general trends governing peptide secondary-structure

stability. Fig. 5(a) shows the MAE values for each FF/water model combination, computed by averaging the absolute deviations from experimental findings. The lowest MAE (11.8%) is obtained with the ff15ipq/TIP4P-D combination. Overall, all FFs combined with 4-site water models show better performance compared to those used with 3-site water models. Among the 3-site water models, acceptable performance is observed with SPC, TIP3P, and TIP3P-EW. Based on the MAE values, ff15ipq and ff199SB-ILDN stand out, followed by ff-FB15. Below-average performances are observed for ff14SB and ff19SB.

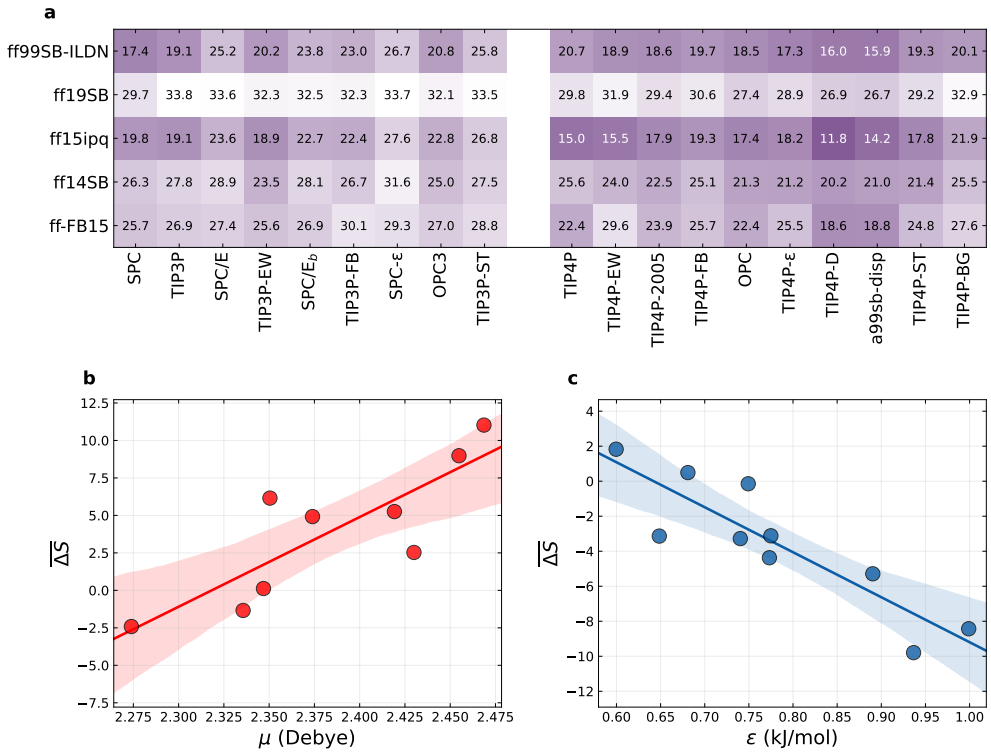


Fig. 5 **a**: Mean Absolute Error (MAE, %) computed for each FF/water model combination, obtained by averaging the absolute deviations from the peptide-specific target values after 20 ns. Lower values indicate better agreement with reference data and are highlighted with a more intense violet color. **b**: Average relative peptide stability ($\overline{\Delta S}$) as a function of the water model dipole (μ) for 3-site water models. **c**: Average relative peptide stability ($\overline{\Delta S}$) as a function of oxygen LJ ϵ parameter for 4-site water models.

Across all FFs and peptide systems examined, a consistent relationship emerges between the effective strength of HB–driven solvent–solvent interactions and the equilibrium between folded and unfolded states. Water models characterized by weaker intrasolvent HBs tend to favor unfolded conformations. Conversely, models with stronger intrasolvent hydrogen bonding tend to stabilize secondary structures. This

trend is observed independently of the specific geometrical details of the water model, indicating that interaction strength plays a more decisive role than molecular geometry *per se*. Notably, however, the mechanistic origin of this overstabilization differs subtly between 3-site and 4-site models, as distinct parameters modulate the effective HB strength in each case. To isolate the effect of the water model on the overstabilization of disordered peptides (H1 and B1), a correlation analysis is performed and summarized in Table S3 and S4 of the SI.

For 3-site water models, $\overline{\Delta S}$ exhibits a strong positive correlation with the molecular dipole moment μ (Fig. 5(b)). Models with reduced partial charges - and therefore weaker water-water HBs - promote unfolding in peptides that are experimentally disordered or only marginally stable. In contrast, experimentally stable sequences (e.g., H2 and B2) show minimal sensitivity to the choice of water model. For disordered peptides, solvent-mediated backbone stabilization is insufficient to compensate for entropic contributions, resulting in enhanced sampling of extended conformations when the solvent HB network is weaker. Conversely, SPC-derived and other optimized 3-site models with larger dipole moments—and thus stronger intrasolvent HBs—artificially reduce the population of unfolded states, promoting an expanded distribution of α-helix or β-sheet content in peptides known experimentally to be disordered. Despite differences in parameterization strategies, these high-dipole models share a common feature: they indirectly enhance intrapeptide HB and backbone contacts, as the highly stable solvent HB network energetically disfavors peptide–solvent HBs, thereby biasing the system toward intramolecular stabilization.

The 4-site water models introduce a more refined electrostatic representation through a massless virtual charge site located along the $\widehat{HOH}$ bisector, while preserving similar O–H geometries across the model family. In these models, variations in the position of the virtual charge and in the LJ parameters modulate the balance between electrostatic and dispersion interactions. In contrast to the 3-site case, secondary-structure overstabilization in H1 and B1 shows only a weak correlation with the molecular dipole moment but a strong anticorrelation with the oxygen LJ ϵ parameter (Fig. 5(c)). Specifically, smaller ϵ values are associated with greater secondary-structure stabilization. This seemingly counterintuitive result can be rationalized by noting that a reduced oxygen ϵ allows closer oxygen–oxygen approach in hydrogen-bonded water pairs, thereby strengthening the electrostatic interaction between the negatively charged virtual site and the hydrogen atom of the partner molecule. Thus, although different parameters control the effect (dipole moment in 3-site models versus oxygen ϵ in 4-site models), the underlying physical mechanism remains the same: excessive strengthening of the intrasolvent HB network indirectly favors intrapeptide hydrogen bonding and secondary-structure formation. These findings are in agreement with the results reported in Ref. [32], where the propensity of the amber03w/TIP4P-2005 combination to overstabilize disordered peptides is mitigated by selectively enhancing the LJ peptide–water interactions through rescaling of the oxygen ϵ parameter.

This analysis demonstrates that subtle tuning of solvent–solvent interactions in water models — independently of the protein FF — plays a key role in modulating the balance between solute–solvent and intramolecular interactions, thereby shaping

peptide conformational behavior. Improvements in the electrostatic representation of water, whether within 3-site or 4-site frameworks, can therefore help mitigate spurious secondary-structure overstabilization observed with many FFs.

The extent to which solvent effects influence peptide conformational equilibrium depends strongly on the underlying FF. FFs such as ff99SB-ILDN, ff-FB15 and ff15ipq exhibit a marked sensitivity to the water model, with large shifts in folded–unfolded populations across different solvent representations. In contrast, ff14SB and ff19SB display a reduced dependence on the choice of water model, consistent with their parametrization strategy that incorporates solvent effects more explicitly through backbone corrections.

Peptide-specific effects further modulate these trends. Sequences unstable in water display a pronounced sensitivity to solvent–solute interaction strength, with substantial changes in secondary-structure populations across different water models. More stable peptides retain a significant degree of secondary structure even in weaker solvents, particularly when combined with FFs that intrinsically favor folded conformations. Nonetheless, the qualitative dependence on solvent interaction strength remains consistent across all sequences examined.

Overall, these results indicate that peptide secondary-structure stability is governed by a continuous balance between FF-encoded backbone preferences and the effective strength of solvent–solute interactions. Water models featuring weaker H-bond networks promote unfolding, whereas models with stronger interactions tend to overstabilize helical conformations. FFs differ in how strongly they amplify or dampen these solvent effects, reflecting differences in parametrization philosophy and target observables. This unified perspective highlights the importance of considering FF and the water model as tightly and subtly intertwined when investigating peptide folding and stability in molecular dynamics simulations.

5 Conclusions

We conducted an extensive benchmark, simulating four peptides (two α-helices and two β-hairpins) with known structural properties in water - ranging from stably folded to random coil - using five popular AMBER FFs paired with 19 different water models. These models span from classic 3-site options, like TIP3P and SPC, to modern 4-site variants, assessing their performance against experimental reference structures. Our study systematically evaluates many FF–water combinations that have not been tested previously, moving beyond established pairings based on convention. This represents a first-of-its-kind assessment of the water model's influence on FF behavior, challenging pairings often based on anecdotal evidence or historical practice.

We find that recent, dihedral-optimized FFs like ff19SB, ff-FB15 and (to a lesser extent) ff14SB - despite careful quantum mechanics–derived parameterization - systematically overestimates the stability of secondary structures in peptides known to be disordered. This overstabilization trend shows little dependency on the choice of the water model, even when deviating from its standard pairing. The most accurate FFs for our benchmark set - correctly predicting two-folded and two mostly unfolded peptides at equilibrium - were the widely used ff99SB-ILDN and ff15ipq. Their best

performance was achieved in combination with 4-site water models such as TIP4P-D, which significantly outperformed their standard pairings with three-site models (TIP3P and SPC/E, respectively).

As a general trend across all FF, water models featuring intrinsically weaker solvent-solvent H-bond networks are less likely to oppose unfolding when it is expected, while still maintaining structure for ordered peptides. Conversely, models yielding a tighter solvent-solvent H-bond matrix (e.g., OPC3, SPC/E) show a tendency to overstabilize secondary structure. While overstabilizing FFs (e.g., ff19SB) show minimal sensitivity to the paired water model, the top performers (ff99SB-ILDN and ff15ipq) exhibit a marked dependency. This highlights the crucial role of a balanced electrostatics model. The ff15ipq FF incorporates refitted, environmentally polarized charges, whereas ff99SB-ILDN relies on in vacuo HF/6-31G RESP charges, which empirically account for solvent polarization. Their superior performance with specific water models underscores the importance of a balanced electrostatic treatment between solute and solvent.

We believe this extensive benchmark - with all data fully available on GitHub - provides valuable guidance for understanding the critical interplay between protein and solvent modeling, offering a data-driven foundation for selecting FF and water model combinations in future biomolecular simulations.

Supplementary information. Figure S1: documents published from 1994 to 2025 that reported the name of one of the most important FFs families. Figure S2: schematic overview of AMBER FF versions and the water models usually used with each FF. Figures S3-S6: information for repository navigation. Figures S7-S11: secondary-structure composition of peptides H1, H2, B1, and B2 obtained from DSSP analysis at the final simulation time using all FFs/water model combinations. Figures S12-S13: analysis of B1 and B2 peptides at higher temperature (340 K). Table S1-S2: parameters of the 3-site and 4-site water models used in the present benchmark. Figure S14: radar plot comparison of geometric and electrostatic parameters for 3-site and 4-site water models. Table S3-S4: multivariate linear regression results.

Acknowledgements. The authors thank MUR-Italy ("Progetto Dipartimenti di Eccellenza 2023-2027" allocated to the Department of Chemistry "Ugo Schiff") and the National Recovery and Resilience Plan, Mission 4 Component 2 - Investment 1.4 - NATIONAL CENTER FOR HPC, BIG DATA AND QUANTUM COMPUTING - funded by the European Union - NextGenerationEU - CUP B83C22002830001.

Data availability

The data that support the findings of this study are openly available in https://doi.org/10.5281/zenodo.18671578 and in https://marinamacchiagodena.github.io/AMBERFFs-WaterModels/.

Competing interests

The authors declare no competing interests.

Author contribution

M.C., M.M., and P.P. conceived and designed the project. M.C. conducted molecular dynamics simulations and data analysis. M.C., M.M., A.M.P., C.A., M.P., and P.P. interpret data. M.C., M.M., A.M.P., C.A., M.P., and P.P. contributed to the writing and proofreading of the paper. M.M. and P.P. supervised and directed the project.

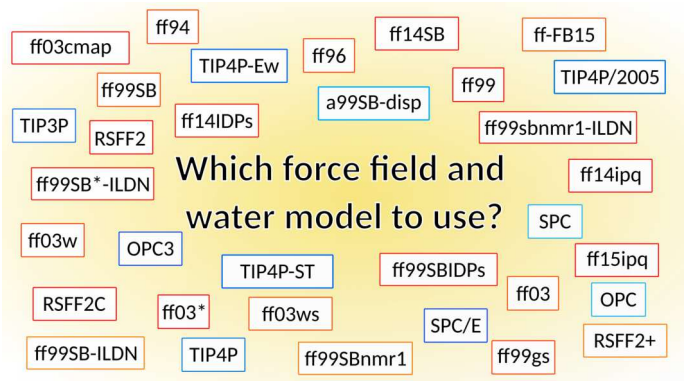


Fig. 6 Graphical Abstract

References

[1] Riniker, S.: Fixed-charge atomistic force fields for molecular dynamics simulations in the condensed phase: An overview. J. Chem. Inf. Model. **58**(3), 565–578 (2018)

[2] Levitt, M., Lifson, S.: Refinement of protein conformations using a macromolecular energy minimization procedure. J. Mol. Biol. **46**(2), 269–279 (1969)

[3] Lifson, S., Warshel, A.: Consistent force field for calculations of conformations, vibrational spectra, and enthalpies of cycloalkane and n-alkane molecules. J. Chem. Phys. **49**(11), 5116–5129 (1968)

[4] Sutcliffe, B.T.: The born-oppenheimer approximation. In: Methods in Computational Molecular Physics, pp. 19–46. Springer, Boston, MA. (1992)

[5] Brooks, C.L., Case, D.A., Plimpton, S., Roux, B., Spoel, D., Tajkhorshid, E.: Classical molecular dynamics. J. Chem. Phys. **154**(10) (2021)

[6] Casoria, M., Macchiagodena, M., Rovero, P., Andreini, C., Papini, A.M., Cardini, G., Pagliai, M.: Upgrading of the general amber force field 2 for fluorinated alcohol biosolvents: A validation for water solutions and melittin solvation. J. Pept. Sci. **30**(2), 3543 (2024)

[7] Casoria, M., Pagliai, M., Andreini, C., Papini, A.M., Procacci, P., Macchiagodena, M.: Fluorinated alcohol biosolvents and α-helix peptide secondary structure: A

molecular dynamics study on the solvent concentration effect. Liquids **6**(1) (2026)

[8] González, M.A.: Force fields and molecular dynamics simulations. École thématique de la Société Française de la Neutronique **12**, 169–200 (2011)

[9] Rizzi, F., Najm, H.N., Debusschere, B.J., Sargsyan, K., Salloum, M., Adalsteinsson, H., Knio, O.M.: Uncertainty quantification in md simulations. part ii: Bayesian inference of force-field parameters. Multiscale Model. Sim. **10**(4), 1460–1492 (2012)

[10] Onufriev, A.V., Izadi, S.: Water models for biomolecular simulations. Wiley Interdiscip. Rev., Comput. Mol. Sci. **8**(2), 1347 (2018)

[11] Pagliai, M., Macchiagodena, M., Procacci, P., Cardini, G.: Evidence of a low–high density turning point in liquid water at ordinary temperature under pressure: A molecular dynamics study. J. Phys. Chem. Lett. **10**(20), 6414–6418 (2019)

[12] Weiner, P.K., Kollman, P.A.: Amber: Assisted model building with energy refinement. a general program for modeling molecules and their interactions. J. Comput. Chem. **2**(3), 287–303 (1981)

[13] Brooks, B.R., Bruccoleri, R.E., Olafson, B.D., States, D.J., Swaminathan, S., Karplus, M.: Charmm: A program for macromolecular energy, minimization, and dynamics calculations. J. Comput. Chem. **4**(2), 187–217 (1983)

[14] Jorgensen, W.L., Tirado-Rives, J.: The opls [optimized potentials for liquid simulations] potential functions for proteins, energy minimizations for crystals of cyclic peptides and crambin. J. Am. Chem. Soc. **110**(6), 1657–1666 (1988)

[15] Scott, W.R.P., Hünenberger, P.H., Tironi, I.G., Mark, A.E., Billeter, S.R., Fennen, J., Torda, A.E., Huber, T., Krüger, P., Gunsteren, W.F.: The gromos biomolecular simulation program package. J. Phys. Chem. A **103**(19), 3596–3607 (1999)

[16] Wang, X., Xiong, D., Zhang, Y., Zhai, J., Gu, Y.-C., He, X.: The evolution of the amber additive protein force field: History, current status, and future. J. Chem. Phys. **162**(3) (2025)

[17] Lindorff-Larsen, K., Piana, S., Palmo, K., Maragakis, P., Klepeis, J.L., Dror, R.O., Shaw, D.E.: Improved side-chain torsion potentials for the amber ff99sb protein force field. Proteins: Struct., Funct., Bioinf. **78**(8), 1950–1958 (2010)

[18] Maier, J.A., Martinez, C., Kasavajhala, K., Wickstrom, L., Hauser, K.E., Simmerling, C.: ff14sb: Improving the accuracy of protein side chain and backbone parameters from ff99sb. J. Chem. Theory Comput. **11**(8), 3696–3713 (2015)

[19] Hornak, V., Abel, R., Okur, A., Strockbine, B., Roitberg, A., Simmerling, C.:

Comparison of multiple amber force fields and development of improved protein backbone parameters. Proteins: Struct., Funct., Bioinf. **65**(3), 712–725 (2006)

[20] Cornell, W.D., Cieplak, P., Bayly, C.I., Gould, I.R., Merz, K.M., Ferguson, D.M., Spellmeyer, D.C., Fox, T., Caldwell, J.W., Kollman, P.A.: A second generation force field for the simulation of proteins, nucleic acids, and organic molecules. J. Am. Chem. Soc. **117**(19), 5179–5197 (1995)

[21] Kollman, P., Dixon, R., Cornell, W., Fox, T., Chipot, C., Pohorille, A.: In: Gunsteren, W.F., Weiner, P.K., Wilkinson, A.J. (eds.) The development/application of a 'minimalist' organic/biochemical molecular mechanic force field using a combination of ab initio calculations and experimental data, pp. 83–96. Springer, Dordrecht (1997)

[22] García, A.E., Sanbonmatsu, K.Y.: α-helical stabilization by side chain shielding of backbone hydrogen bonds. Proc. Natl. Acad. Sci. U.S.A. **99**(5), 2782–2787 (2002)

[23] Wang, L.-P., McKiernan, K.A., Gomes, J., Beauchamp, K.A., Head-Gordon, T., Rice, J.E., Swope, W.C., Martínez, T.J., Pande, V.S.: Building a more predictive protein force field: A systematic and reproducible route to amber-fb15. J. Phys. Chem. B. **121**(16), 4023–4039 (2017)

[24] Cerutti, D.S., Swope, W.C., Rice, J.E., Case, D.A.: ff14ipq: A self-consistent force field for condensed-phase simulations of proteins. J. Chem. Theory Comput. **10**(10), 4515–4534 (2014)

[25] Debiec, K.T., Cerutti, D.S., Baker, L.R., Gronenborn, A.M., Case, D.A., Chong, L.T.: Further along the road less traveled: Amber ff15ipq, an original protein force field built on a self-consistent physical model. J. Chem. Theory Comput. **12**(8), 3926–3947 (2016)

[26] Wang, J., Cieplak, P., Kollman, P.A.: How well does a restrained electrostatic potential (resp) model perform in calculating conformational energies of organic and biological molecules? J. Comput. Chem. **21**(12), 1049–1074 (2000)

[27] Sorin, E.J., Pande, V.S.: Exploring the helix-coil transition via all-atom equilibrium ensemble simulations. Biophys. J. **88**(4), 2472–2493 (2005)

[28] Duan, Y., Wu, C., Chowdhury, S., Lee, M.C., Xiong, G., Zhang, W., Yang, R., Cieplak, P., Luo, R., Lee, T., Caldwell, J., Wang, J., Kollman, P.: A point-charge force field for molecular mechanics simulations of proteins based on condensed-phase quantum mechanical calculations. J. Comput. Chem. **24**(16), 1999–2012 (2003)

[29] Best, R.B., Mittal, J.: Protein simulations with an optimized water model: Cooperative helix formation and temperature-induced unfolded state collapse. J. Phys.

Chem. B. **114**(46), 14916–14923 (2010)

[30] Best, R.B., Hummer, G.: Optimized molecular dynamics force fields applied to the helix coil transition of polypeptides. J. Phys. Chem. B. **113**(26), 9004–9015 (2009)

[31] Zhang, Y., Liu, H., Yang, S., Luo, R., Chen, H.-F.: Well-balanced force field ff03cmap for folded and disordered proteins. J. Chem. Theory Comput. **15**(12), 6769–6780 (2019)

[32] Best, R.B., Zheng, W., Mittal, J.: Balanced protein–water interactions improve properties of disordered proteins and non-specific protein association. J. Chem. Theory Comput. **10**(11), 5113–5124 (2014)

[33] Nerenberg, P.S., Head-Gordon, T.: Optimizing protein solvent force fields to reproduce intrinsic conformational preferences of model peptides. J. Chem. Theory Comput. **7**(4), 1220–1230 (2011)

[34] Zhou, C.-Y., Jiang, F., Wu, Y.-D.: Residue-specific force field based on protein coil library. rsff2: Modification of amber ff99sb. J. Phys. Chem. B. **119**(3), 1035–1047 (2015)

[35] Kang, W., Jiang, F., Wu, Y.-D.: Universal implementation of a residue-specific force field based on cmap potentials and free energy decomposition. J. Chem. Theory Comput. **14**(8), 4474–4486 (2018)

[36] Wu, H.-N., Jiang, F., Wu, Y.-D.: Significantly improved protein folding thermodynamics using a dispersion-corrected water model and a new residue-specific force field. J. Phys. Chem. Lett. **8**(14), 3199–3205 (2017)

[37] Li, D.-W., Brüschweiler, R.: Nmr-based protein potentials. Angew. Chem. Int. Ed. **49**(38), 6778–6780 (2010)

[38] Yu, L., Li, D.-W., Brüschweiler, R.: Balanced amino-acid-specific molecular dynamics force field for the realistic simulation of both folded and disordered proteins. J. Chem. Theory Comput. **16**(2), 1311–1318 (2020)

[39] Best, R.B., Sancho, D., Mittal, J.: Residue-specific α-helix propensities from molecular simulation. Biophys. J. **102**(6), 1462–1467 (2012)

[40] Wang, W., Ye, W., Jiang, C., Luo, R., Chen, H.-F.: New force field on modeling intrinsically disordered proteins. Chem. Biol. Drug Des. **84**(3), 253–269 (2014)

[41] Robustelli, P., Piana, S., Shaw, D.E.: Developing a molecular dynamics force field for both folded and disordered protein states. Proc. Natl. Acad. Sci. U.S.A. **115**(21), 4758–4766 (2018)

[42] Piana, S., Robustelli, P., Tan, D., Chen, S., Shaw, D.E.: Development of a force

field for the simulation of single-chain proteins and protein–protein complexes. J. Chem. Theory Comput. **16**(4), 2494–2507 (2020)

[43] Tian, C., Kasavajhala, K., Belfon, K.A.A., Raguette, L., Huang, H., Migues, A.N., Bickel, J., Wang, Y., Pincay, J., Wu, Q., Simmerling, C.: ff19sb: Amino-acid-specific protein backbone parameters trained against quantum mechanics energy surfaces in solution. J. Chem. Theory Comput. **16**(1), 528–552 (2020)

[44] Suresh, A., Schweitzer-Stenner, R., Urbanc, B.: Amber ff24exp-ga, based on empirical ramachandran distributions of glycine and alanine residues in water. J. Chem. Theory Comput. **21**(5), 2515–2534 (2025)

[45] Song, D., Wang, W., Ye, W., Ji, D., Luo, R., Chen, H.-F.: ff14idps force field improving the conformation sampling of intrinsically disordered proteins. Chem. Biol. Drug Des. **89**(1), 5–15 (2017)

[46] Song, D., Luo, R., Chen, H.-F.: The idp-specific force field ff14idpsff improves the conformer sampling of intrinsically disordered proteins. J. Chem. Inf. Model. **57**(5), 1166–1178 (2017)

[47] Song, D., Liu, H., Luo, R., Chen, H.-F.: Environment-specific force field for intrinsically disordered and ordered proteins. J. Chem. Inf. Model. **60**(4), 2257–2267 (2020)

[48] Kadaoluwa Pathirannahalage, S.P., Meftahi, N., Elbourne, A., Weiss, A.C., McConville, C.F., Padua, A., Winkler, D.A., Costa Gomes, M., Greaves, T.L., Le, T.C., *et al.*: Systematic comparison of the structural and dynamic properties of commonly used water models for molecular dynamics simulations. J. Chem. Inf. Model. **61**(9), 4521–4536 (2021)

[49] Vega, C., Abascal, J.L.: Simulating water with rigid non-polarizable models: a general perspective. Phys. Chem. Chem. Phys. **13**(44), 19663–19688 (2011)

[50] Sedano, L., Blazquez, S., Vega, C.: Accuracy limit of non-polarizable four-point water models: Tip4p/2005 vs opc. should water models reproduce the experimental dielectric constant? J. Chem. Phys. **161**(4) (2024)

[51] Hornak, V., Abel, R., Okur, A., Strockbine, B., Roitberg, A., Simmerling, C.: Comparison of multiple amber force fields and development of improved protein backbone parameters. Proteins: Struct., Funct., Bioinf. **65**(3), 712–725 (2006)

[52] Thompson, E.J., DePaul, A.J., Patel, S.S., Sorin, E.J.: Evaluating molecular mechanical potentials for helical peptides and proteins. PLoS One **5**(4), 10056 (2010)

[53] Fischer, A.-L.M., Tichy, A., Kokot, J., Hoerschinger, V.J., Wild, R.F., Riccabona, J.R., Loeffler, J.R., Waibl, F., Quoika, P.K., Gschwandtner, P., *et al.*: The role

of force fields and water models in protein folding and unfolding dynamics. J. Chem. Theory Comput. **20**(5), 2321–2333 (2024)

[54] Zhang, H., Yin, C., Jiang, Y., Spoel, D.: Force field benchmark of amino acids: I. hydration and diffusion in different water models. J. Chem. Inf. Model. **58**(5), 1037–1052 (2018)

[55] Beauchamp, K.A., Lin, Y.-S., Das, R., Pande, V.S.: Are protein force fields getting better? a systematic benchmark on 524 diverse nmr measurements. J. Chem. Theory Comput. **8**(4), 1409–1414 (2012)

[56] Berendsen, H.J.C., Postma, J.P.M., Gunsteren, W.F., Hermans, J.: In: Pullman, B. (ed.) Interaction Models for Water in Relation to Protein Hydration, pp. 331–342. Springer, Dordrecht (1981)

[57] Jorgensen, W.L., Chandrasekhar, J., Madura, J.D., Impey, R.W., Klein, M.L.: Comparison of simple potential functions for simulating liquid water. J. Chem. Phys. **79**(2), 926–935 (1983)

[58] Berendsen, H.J.C., Grigera, J.R., Straatsma, T.P.: The missing term in effective pair potentials. J. Phys. Chem. **91**(24), 6269–6271 (1987)

[59] Price, D.J., Brooks, I. Charles L.: A modified tip3p water potential for simulation with ewald summation. J. Chem. Phys. **121**(20), 10096–10103 (2004)

[60] Takemura, K., Kitao, A.: Water model tuning for improved reproduction of rotational diffusion and nmr spectral density. J. Phys. Chem. B. **116**(22), 6279–6287 (2012)

[61] Wang, L.-P., Martinez, T.J., Pande, V.S.: Building force fields: An automatic, systematic, and reproducible approach. J. Phys. Chem. Lett. **5**(11), 1885–1891 (2014)

[62] Fuentes-Azcatl, R., Mendoza, N., Alejandre, J.: Improved spc force field of water based on the dielectric constant: Spc/ϵ. Phys. A: Stat. Mech. Appl. **420**, 116–123 (2015)

[63] Izadi, S., Onufriev, A.V.: Accuracy limit of rigid 3-point water models. J. Chem. Phys **145**(7), 074501 (2016)

[64] Qiu, Y., Nerenberg, P.S., Head-Gordon, T., Wang, L.-P.: Systematic optimization of water models using liquid/vapor surface tension data. J. Phys. Chem. B. **123**(32), 7061–7073 (2019)

[65] Vega, C., Abascal, J.L.F., Nezbeda, I.: Vapor-liquid equilibria from the triple point up to the critical point for the new generation of tip4p-like models: Tip4p/ew, tip4p/2005, and tip4p/ice. J. Chem. Phys. **125**(3), 034503 (2006)

[66] Abascal, J.L.F., Vega, C.: A general purpose model for the condensed phases of water: Tip4p/2005. J. Chem. Phys. **123**(23), 234505 (2005)

[67] Izadi, S., Anandakrishnan, R., Onufriev, A.V.: Building water models: A different approach. J. Phys. Chem. Lett. **5**(21), 3863–3871 (2014)

[68] Fuentes-Azcatl, R., Alejandre, J.: Non-polarizable force field of water based on the dielectric constant: Tip4p/ϵ. J. Phys. Chem. B. **118**(5), 1263–1272 (2014)

[69] Piana, S., Donchev, A.G., Robustelli, P., Shaw, D.E.: Water dispersion interactions strongly influence simulated structural properties of disordered protein states. J. Phys. Chem. B. **119**(16), 5113–5123 (2015)

[70] Ye, H.-f., Wang, J., Zheng, Y.-g., Zhang, H.-w., Chen, Z.: Machine learning for reparameterization of four-site water models: Tip4p-bg and tip4p-bgt. Phys. Chem. Chem. Phys. **23**, 10164–10173 (2021)

[71] Montserret, R., McLeish, M.J., Böckmann, A., Geourjon, C., Penin, F.: Involvement of electrostatic interactions in the mechanism of peptide folding induced by sodium dodecyl sulfate binding. Biochemistry **39**(29), 8362–8373 (2000)

[72] Neidigh, J.W., Fesinmeyer, R.M., Andersen, N.H.: Designing a 20-residue protein. Nat. Struct. Biol. **9**(6), 425–430 (2002)

[73] Gronenborn, A.M., Filpula, D.R., Essig, N.Z., Achari, A., Whitlow, M., Wingfield, P.T., Clore, G.M.: A novel, highly stable fold of the immunoglobulin binding domain of streptococcal protein g. Science **253**(5020), 657–661 (1991)

[74] Blanco, F.J., Jimenez, M.A., Pineda, A., Rico, M., Santoro, J., Nieto, J.L.: Nmr solution structure of the isolated n-terminal fragment of protein-g b1 domain. evidence of trifluoroethanol induced native-like .beta.-hairpin formation. Biochemistry **33**(19), 6004–6014 (1994)

[75] Blanco, F.J., Rivas, G., Serrano, L.: A short linear peptide that folds into a native stable β-hairpin in aqueous solution. Nat. Struct. Biol. **1**(9), 584–590 (1994)

[76] Muñoz, V., Thompson, P.A., Hofrichter, J., Eaton, W.A.: Folding dynamics and mechanism of β-hairpin formation. Nature **390**(6656), 196–199 (1997)

[77] Lorentz, H.A.: Ueber die anwendung des satzes vom virial in der kinetischen theorie der gase. Ann. Phys. **248**, 127–136 (1881)

[78] Berthelot, D.: Sur le melange des gaz. Compt. Rend. Hebd. Séances Acad. Sci. **126**, 1703–1855 (1898)

[79] Bhati, A.P., Wan, S., Hu, Y., Sherborne, B., Coveney, P.V.: Uncertainty quantification in alchemical free energy methods. J. Chem. Theory Comput. **14**(6), 2867–2880 (2018)

[80] Procacci, P.: Dealing with induced fit, conformational selection, and secondary poses in molecular dynamics simulations for reliable free energy predictions. J. Chem. Theory Comput. **19**(23), 8942–8954 (2023)

[81] Coveney, P.V., Wan, S.: On the calculation of equilibrium thermodynamic properties from molecular dynamics. Phys. Chem. Chem. Phys. **18**(44), 30236–30240 (2016)

[82] Abraham, M.J., Murtola, T., Schulz, R., Páll, S., Smith, J.C., Hess, B., Lindahl, E.: Gromacs: High performance molecular simulations through multi-level parallelism from laptops to supercomputers. SoftwareX **1-2**, 19–25 (2015)

[83] Case, D.A., Aktulga, H.M., Belfon, K., Cerutti, D.S., Cisneros, G.A., Cruzeiro, V.W.D., Forouzesh, N., Giese, T.J., Götz, A.W., Gohlke, H., Izadi, S., Kasavajhala, K., Kaymak, M.C., King, E., Kurtzman, T., Lee, T.-S., Li, P., Liu, J., Luchko, T., Luo, R., Manathunga, M., Machado, M.R., Nguyen, H.M., O'Hearn, K.A., Onufriev, A.V., Pan, F., Pantano, S., Qi, R., Rahnamoun, A., Risheh, A., Schott-Verdugo, S., Shajan, A., Swails, J., Wang, J., Wei, H., Wu, X., Wu, Y., Zhang, S., Zhao, S., Zhu, Q., Cheatham, T.E.I., Roe, D.R., Roitberg, A., Simmerling, C., York, D.M., Nagan, M.C., Merz, K.M.J.: Ambertools. J. Chem. Inf. Model. **63**(20), 6183–6191 (2023)

[84] Shirts, M.R., Klein, C., Swails, J.M., Yin, J., Gilson, M.K., Mobley, D.L., Case, D.A., Zhong, E.D.: Lessons learned from comparing molecular dynamics engines on the sampl5 dataset. J. Comput. Aided Mol. Des. **31**(1), 147–161 (2017)

[85] Bussi, G., Donadio, D., Parrinello, M.: Canonical sampling through velocity rescaling. J. Chem. Phys. **126**(1), 014101 (2007)

[86] Hess, B., Bekker, H., Berendsen, H.J., Fraaije, J.G.: Lincs: a linear constraint solver for molecular simulations. J. Comput. Chem. **18**(12), 1463–1472 (1997)

[87] Darden, T., York, D., Pedersen, L.: Particle mesh ewald: An n·log (n) method for ewald sums in large systems. J. Chem. Phys. **98**(12), 10089–10092 (1993)

[88] Allen, M.P., Tildesley, D.J.: Computer Simulation of Liquids. Press, Oxford Clarendon, Oxford (1987)

[89] Kabsch, W., Sander, C.: Dictionary of protein secondary structure: Pattern recognition of hydrogen-bonded and geometrical features. Biopolymers **22**(12), 2577–2637 (1983)

[90] Hekkelman, M.L., Salmoral, D.Á., Perrakis, A., Joosten, R.P.: Dssp 4: Fair annotation of protein secondary structure. Protein Science **34**(8), 70208 (2025)

[91] Seabold, S., Perktold, J.: Statsmodels: Econometric and statistical modeling with python. In: 9th Python in Science Conference (2010)

Supplementary Files

This is a list of supplementary files associated with this preprint. Click to download.

- SI.pdf